Application of the Manifold Cell Model in Rainfall-Runoff Analysis of a Hydrologic System

AUTHOR(S):

WANG, Ru-yih; IKEBUCHI, Shuichi

CITATION:

WANG, Ru-yih ...[et al]. Application of the Manifold Cell Model in Rainfall-Runoff Analysis of a Hydrologic System. Bulletin of the Disaster Prevention Research Institute 1994, 44(2): 93-121

ISSUE DATE:

1994-06

URL:

http://hdl.handle.net/2433/125000

Bull. Disas. Prev. Res. Inst., Kyoto Univ., Vol. 44, Part 2, No. 381, June, 1994

Application of the Manifold Cell Model in Rainfall-Runoff Analysis of a Hydrologic System

By Ru-yih WANG and Shuichi IKEBUCHI

(Manuscript recieved on June 25, 1994, revised on August 19, 1994)

Abstract

The paper aims to modify the newly developed manifold cell model, then to build up adequate rainfall-runoff model for simulating the spatially distributed characteristics of a hydrologic system, and finally, to apply the model for flood forecasting so as to predict accurately and instantaneously the possible flood trend in a river basin during typhoon hitting period. In order to verify the accuracy of the manifold cell model, Tseng-wen River Basin, Taiwan was chosen as a project area for illustration. From the analyzed results, the proposed manifold cell model was found to be proper for applying to the simulation of the deterministic relationship between rainfall and runoff.

1. Introduction

Hydrologic modeling is a mathematical formulation by which appropriate governing equations to study the relationship of cause and effect in a hydrologic system are set up. Hydrologic phenomenon occurring in a river basin usually varies with respect to time and space (2, 3, 11). The time base and spatial extent of a hydrologic model will reflect both the modeling objectives and the degrees of realism sought in the model. If a river basin is regarded as a lumped system, all the hydrologic variables are treated as constant in space. As a result, characteristics of spatial non-uniformity among meteorologic components, hydrologic parameters and physiographic factors are commonly neglected. On the other hand, distributed model considers the characteristics of spatial variation in a real and complicated river basin, leading to complexity in model structure. A distributed model has a wide application especially for those project areas which have abrupt weather changes, flashy flood variations and rugged topographic situation.

Distributed models place more emphasis on the particular situation such as irregular changes of hydrologic condition and great spatial variation of physiographic situation. Some examples of applicable distributed models are: (1) isochrone routing model, originally proposed by Clark in 1945, which is based on time-area diagram of a watershed as a weighting input function routing from the upstream component to the outlet (6, 13). (2) geomorphologic instantaneous unit hydrograph model (GIUH), which is a physically-distributed model developed by means of the queuing theory. Based upon the data accumulation from topographic maps of a project basin, a GIUH can be built up for flood estimation (12). (3) topographic basin model, proposed by

Takasao and Shiiba in 1989, which is a numerical model for taking account of the direction of water flow. A topographic surface is numerically represented using a data structure of Digital Elevation Model (DEM) formed by a Triangulated Irregular Network (TIN). Land surfaces are modeled as a set of contiguous non-overlapping triangular facets whose vertices are made up by points on regular grids and points on river segments (9). (4) cell model which is a conceptually distributed model that divides a watershed into several adequate subareas or cell according to respective topographic character. The characteristics of spatial variation of topography can be revealed in the cell model if a spatially uniform rainfall falls on a river basin.

The aims of this paper are firstly to discuss and modify the impulse response functions of manifold cell model, secondly to build up suitable hydrologic model for simulating the spatially distributed characteristics of a river system, and finally, to apply the modeling results for flood prediction.

2. Discussion and Modification of Impulse Response Function for the Manifold Cell Model

Impulse response function (IRF) is defined as the resulting outflow at the outlet of a river basin by adding instantaneously an unit depth of rainfall excess into a hydrologic system. It is conceptually similar to the instantaneous unit hydrograph. In this study, hydrologic phenomena occurring in a cell are assumed to be linear processes. Regarding rainfall excess as inflow to the cell, by means of operation with IRF of the cell, the resulting outflow hydrograph at the outlet of a river basin can be routed in sequence by applying the principle of convolution.

The structure of the manifold cell model is composed of two cascaded linear reservoirs. The first element is a linear reservoir of storage constant k_a to simulate the effect of overland flow; the second element is another linear reservoir of storage constant of i^{th} cell $i \cdot k_m$ ($i=1,2,\cdots,n$, n: number of cells), to simulate the channel effect as shown in **Fig. 1**. From **Fig. 1**(B), the longer the distance to the outlet, the larger the storage constant of a channel is, and the longer the time lag becomes. As a result, the IRF of i^{th} cell to the outlet can be obtained by applying the principle of convolution as:

$$g_i(t)=\frac{1}{n}\int_0^t \frac{1}{k_a} e^{-\frac{t-v}{k_a}} \cdot \frac{1}{ik_m} e^{-\frac{v}{ik_m}} dv$$

$$=\frac{1}{n}\cdot\frac{1}{k_a-ik_m}\left(e^{-\frac{t}{k_a}}-e^{-\frac{t}{ik_m}}\right) \tag{1}$$

Summating eq. (1) for $i=1,2,\cdots,n$, $h_n(t)$ can be expressed as:

$$h_n(t)=\sum_{i=1}^{n} g_i(t)$$

$$=\frac{1}{n}\sum_{i=1}^{n}\frac{1}{k_a-ik_m}\left(e^{-\frac{t}{k_a}}-e^{-\frac{t}{ik_m}}\right) \tag{2}$$

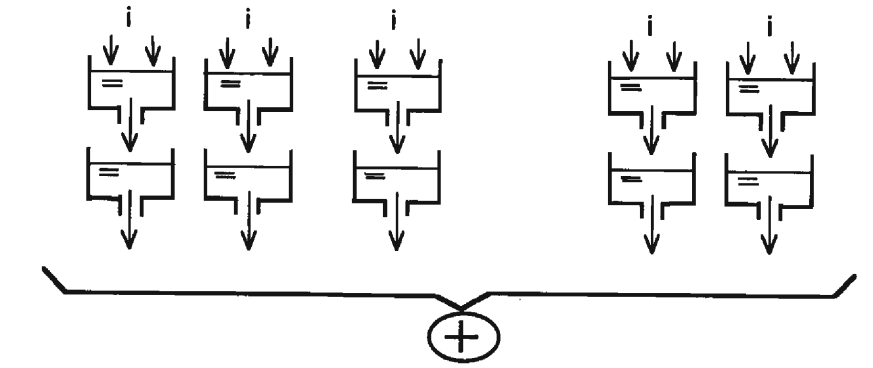

(A) Conceptual model of linear reservoirs.

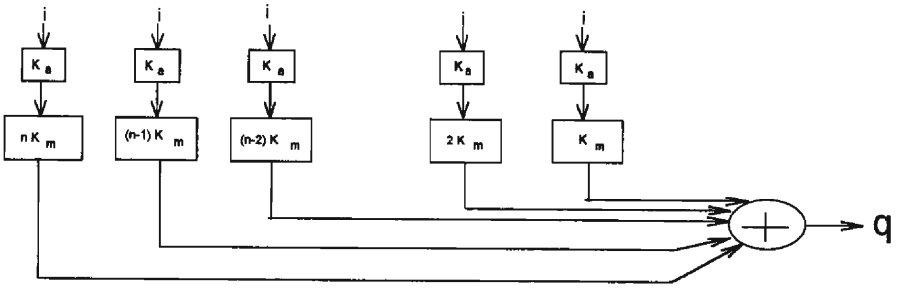

(B) Systematic block diagram.

Fig. 1. Diagram of the manifold cell model.

where, $h_n(t)$ is the IRF for whole river basin.

Taking the Laplace transform of eqs. (1) and (2) yields:

$$G_i(s)=L\{g_i(t)\}$$

$$=\frac{1}{n}\cdot\frac{1}{1+k_a s}\cdot\frac{1}{1+ik_m s} \tag{3}$$

and $H_n(s)=\sum_{i=1}^{n} G_i(s)$

$$=\frac{1}{n}\cdot\frac{1}{1+k_a s}\sum_{i=1}^{n}\frac{1}{1+ik_m s} \tag{4}$$

Taking the first moment of $h_n(t)$ as the first derivative of $H_n(s)$ at $s=0$, so

$$M_n=-\left.\frac{dH_n(s)}{ds}\right|_{s=0}$$

$$=k_a+\frac{(n+1)k_m}{2} \tag{5}$$

Let $M=L-k_a$, where $L=M_n$ represents time lag, then

$$k_m=\frac{2M}{n+1} \tag{6}$$

Substituting eq. (6) into eq. (4) yields:

$$H_n(s)=\frac{1}{n}\sum_{i=1}^{n}\frac{1}{1+k_a s}\cdot\frac{1}{1+\frac{2Mis}{n+1}} \tag{7}$$

When $n\to\infty$, then

$$\lim_{n\to\infty} H_n(s)=\frac{1}{1+k_a s}\lim_{n\to\infty}\frac{1}{n}\sum_{i=1}^{n}\frac{1}{1+\frac{2Mis}{n+1}} \tag{8}$$

Here, $\frac{1}{n}\sum_{i=1}^{n}\frac{1}{1+ib}=\frac{1}{n}\sum_{i=1}^{n}[1-ib+(ib)^2-(ib)^3+-\cdots\cdots]$

$$=\frac{1}{n}\left[n-\frac{n(n+1)}{2}b+\frac{n(n+1)\left(n+\frac{1}{2}\right)}{3}b^2-\frac{n^2(n+1)^2}{4}b^3+-\cdots\cdots\right] \tag{9}$$

where, $b=\frac{2Ms}{n+1}$.

Substituting eq. (9) into eq. (8) obtains:

$$\lim_{n\to\infty} H_n(s)=\frac{1}{1+k_a s}\frac{1}{2Ms}\left[2Ms-\frac{(2Ms)^2}{2}+\frac{(2Ms)^3}{3}-+\cdots\cdots\right]$$

$$=\frac{1}{1+k_a s}\frac{1}{2Ms}\ln(1+2Ms) \tag{10}$$

Taking the inverse Laplace transform of eq. (10) yields:

$$h(t)=L^{-1}\{\lim_{n\to\infty} \mathrm{H_n}(s)\}$$

$$=L^{-1}\left\{\frac{1}{1+k_a s}\cdot\frac{1}{2Ms}\ln(1+2Ms)\right\} \tag{11}$$

in which, $L^{-1}\left\{\frac{1}{2Ms}\cdot\ln(1+2Ms)\right\}=E_1\left(\frac{t}{2M}\right)$

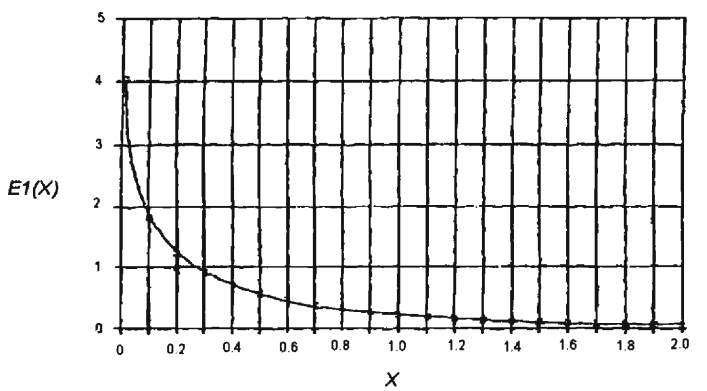

Fig. 2. Illustration of the exponential integral function.

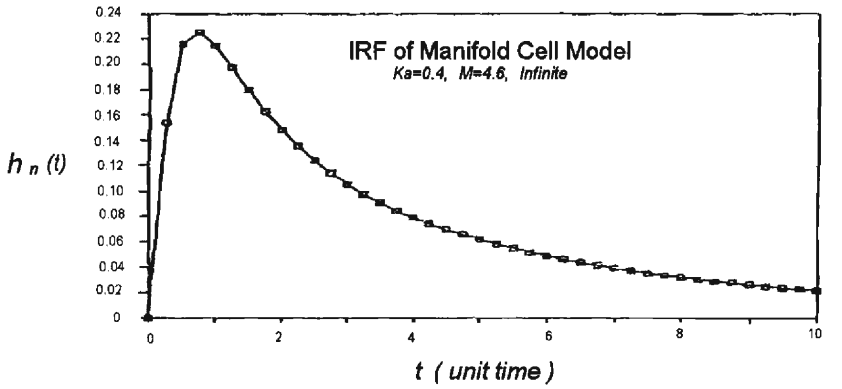

Fig. 3. Impulse response function of the manifold cell model. (K_a=0.4, M=4.6, n=∞)

where, $E_1\left(\frac{t}{2M}\right)$ is the exponential integral function, and its shape is drawn in **Fig. 2**. Hence eq. (11) can be modified as:

$$h(t)=\int_0^t \frac{1}{k_a} e^{-\frac{t-v}{k_a}} E_1\left(\frac{v}{2M}\right)dv \tag{12}$$

Because no analytical solution can be obtained for eq. (12), method of numerical integration by applying Simpson's 1/3 rule is adopted. Setting time lag $L=5$, $k_a=0.4$, $M=L-k_a=4.6$ and integrating for numerical solution, the result of IRF can be shown as **Fig. 3**. It can be seen from **Fig. 3** that IRF of the manifold cell model is quite similar to the typical shape of IUH. Theoretically, the manifold cell model is a distributed model if the number of subareas becomes large enough. For determining the number of divisions of a river basin for practical application, numerical tests are carried out by the following two groups:

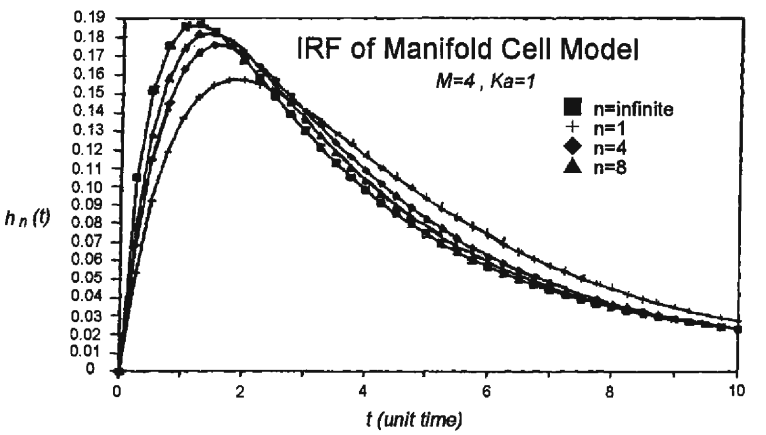

Fig. 4. Impulse response function of the manifold cell model. (K_a=1, M=4)

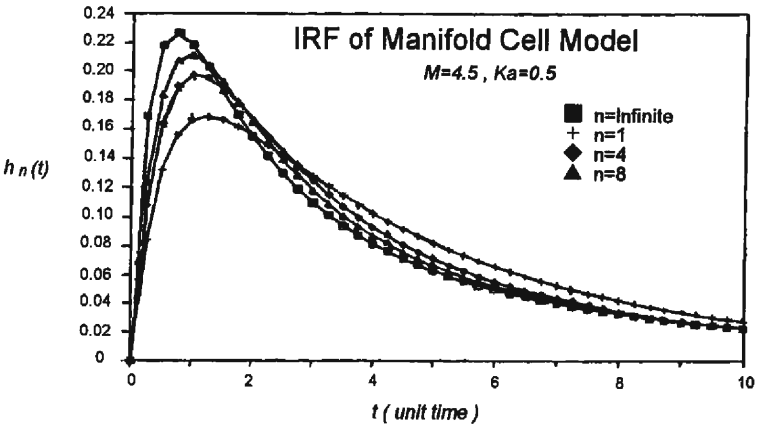

Fig. 5. Impulse response function of the manifold cell model. (K_a=0.5, M=4.5)

Group 1 Let$L$=5, k_a=1.0, M=4.0, then IRF is from eqs. (2) and (6)

$$h_n(t)=\frac{1}{n}\sum_{i=1}^{n}\frac{1}{1-\frac{8i}{n+1}}\left(e^{-\frac{t}{1.0}}-e^{-\frac{t}{\frac{8i}{n+1}}}\right) \tag{13}$$

the functional figure of eq. (13) is shown as in **Fig. 4.**

Group 2 Let$L$=5, k_a=0.5, M=4.5, then IRF is

$$h_n(t)=\frac{1}{n}\sum_{i=1}^{n}\frac{1}{0.5-\frac{9i}{n+1}}\left(e^{-\frac{t}{0.5}}-e^{-\frac{t}{\frac{9i}{n+1}}}\right) \tag{14}$$

the functional figure of eq. (14) is plotted as in **Fig. 5.**

The results of numerical tests from eqs. (13) and (14) are summarized in **Table 1.**

Table 1. Result of numerical test of the manifold cell model

number of cells	*M* 4.5 *Ka* 0.5 *L* 5.0		*M* 4.0 *Ka* 1.0 *L* 5.0	
	ratio of time to peak	ratio of peak discharge	ratio of time to peak	ratio of peak discharge
1	1.67	0.73	1.40	0.84
2	1.67	0.80	1.40	0.89
4	1.33	0.87	1.20	0.94
8	1.33	0.93	1.20	0.98
16	1.00	0.97	1.00	0.99
32	1.00	0.99	1.00	1.00
64	1.00	1.00	1.00	1.00
128	1.00	1.00	1.00	1.00
256	1.00	1.00	1.00	1.00

It can be seen that the ratio of time to peak and the ratio of peak discharge become unity when the number of divisions of a river basin, n is large enough. The ratio of time to peak remains as one and the error of the ratio of peak discharge is 3% when n is 16. As a result, $n=16$ or so is appropriate for practical flood estimation when applying the manifold cell model.

3. Modification of the Manifold Cell Model by ARX Scheme

Manifold cell model was originally proposed by Diskin in 1987 (4, 8, 9). Similar hydrologic characteristic is assumed in each cell. An adequate flow network can be constructed according to the flow pattern occurred in the mechanism of a river basin (7). The deterministic relationship between rainfall and runoff can be finally simulated by connecting cells and formed as a cell model. Because the varying physiographic factors in each cell are considered, the manifold cell model can be regarded as a distributed model.

Modification of the manifold cell model by applying the scheme of an autoregressive model with exogenous input (or simply ARX model) is proposed herein. As shown in **Fig. 1**, components of overland flow and streamflow can be individually derived in the manifold cell model.

3.1 Overland Flow

Let us consider the equation of continuity of j^{th} cell as:

$$I_j(t)-Q_{1,j}(t)=\frac{dS_{1,j}(t)}{dt} \tag{15}$$

where, $I_j(t)$: input function of j^{th} cell, cms;
$Q_{1,j}(t)$: overland flow of j^{th} cell, cms;
$S_{1,j}(t)$: storage of overland flow of j^{th} cell, m^3.

Substituting $S_{1,j}(t)=k_aQ_{1,j}(t)$ into eq. (15) obtains:

$$I_j(t)-\frac{1}{k_a}S_{1,j}(t)=\frac{dS_{1,j}(t)}{dt} \tag{16}$$

Integrating the above equation from $t-1$ to t by applying the trapezoidal rule, we get:

$$\frac{1}{2}(1+B)I_j(t)-\frac{1}{2k_a}(1+B)S_{1,j}(t)=S_{1,j}(t)(1-B) \tag{17}$$

where, B: backshift operator,

$$\text{thus}\quad \left[(1-B)+\frac{1}{2k_a}(1+B)\right]S_{1,j}(t)=\frac{1}{2}(1+B)I_j(t) \tag{18}$$

Let $\alpha_1=-\left(1-\frac{1}{2k_a}\right)$, $\alpha_2=1+\frac{1}{2k_a}$, then eq. (18) can be rewritten as:

$$[\alpha_2+\alpha_1B]S_{1,j}(t)=\frac{1}{2}(1+B)I_j(t) \tag{19}$$

$$\text{or} \quad S_{1,j}(t)=\frac{\frac{1}{2}(1+B)}{[\alpha_2+\alpha_1 B]}I_j(t) \tag{20}$$

3.2 Streamflow

The equation of continuity for the streamflow part can be expressed as:

$$Q_{1,j}(t)-Q_{2,j}(t)=\frac{dS_{2,j}(t)}{dt} \tag{21}$$

where, $Q_{2,j}(t)$ represents streamflow discharge of j^{th} cell, cms and $S_{2,j}(t)$ is storage of streamflow of j^{th} cell, m^3.

Substituting the relation $S_{2,j}(t)=M_jQ_{2,j}(t)$ into eq. (21), where M_j is the storage constant of streamflow for the j^{th} cell, we have:

$$\frac{1}{k_a}S_{1,j}(t)-\frac{1}{M_j}S_{2,j}(t)=\frac{dS_{2,j}(t)}{dt} \tag{22}$$

Integrating the above equation from $t-1$ to t by applying the trapezoidal rule and yields:

$$\frac{1}{2k_a}(1+B)S_{1,j}(t)-\frac{1}{2M_j}(1+B)S_{2,j}(t)=(1-B)S_{2,j}(t) \tag{23}$$

$$\text{or} \quad \left[(1-B)+\frac{1}{2M_j}(1+B)\right]S_{2,j}(t)=\frac{1}{2k_a}(1+B)S_{1,j}(t) \tag{24}$$

Let $\beta_1=-\left(1-\frac{1}{2M_j}\right)$, $\beta_2=1+\frac{1}{2M_j}$, and substituting the result of eq. (20) into eq. (24) yields:

$$(\beta_2+\beta_1 B)S_{2,j}(t)=\frac{1}{2k_a}(1+B)\frac{\frac{1}{2}(1+B)I_j(t)}{\alpha_2+\alpha_1 B} \tag{25}$$

$$\text{or} \quad S_{2,j}(t)=\frac{\frac{1}{4k_a}(1+B)^2}{(\alpha_2+\alpha_1 B)(\beta_2+\beta_1 B)}I_j(t) \tag{26}$$

$$\text{thus} \quad Q_{2,j}(t)=\frac{1}{4k_aM_j}\frac{1+2B+B^2}{(\alpha_2\beta_2+\alpha_1\beta_2 B+\alpha_2\beta_1 B+\alpha_1\beta_1 B^2)}I_j(t) \tag{27}$$

Extension of eq. (27) in ARX form yields:

$$Q_{2,j}(t)=-\phi_{1,j}Q_{2,j}(t-1)-\phi_{2,j}Q_{2,j}(t-2)+\theta_{0,j}I_j(t)+\theta_{1,j}\cdot Ij(t-1)+\theta_{2,j}I_j(t-2) \tag{28}$$

in which,

$$\phi_{1,j}=-\frac{(2k_a-1)(2M_j+1)+(2k_a+1)(2M_j-1)}{(2k_a+1)(2M_j+1)},\quad \phi_{2,j}=\frac{(2k_a-1)(2M_j-1)}{(2k_a+1)(2M_j+1)}$$

$$\theta_{o,j}=\frac{1}{(2k_a+1)(2M_j+1)},\quad \theta_{1,j}=2\theta_{0,j},\quad \theta_{2,j}=\theta_{0,j}$$

and furthermore, for $k_a \geq 1$, $M_j \geq 1$, these parameters range as follows:

$$-2 < \phi_{1,j} < -\frac{2}{3},\ -\frac{1}{9} < \phi_{2,j} < 1,\ 0 < \theta_{0,j} \leq \frac{1}{9},\ 0 < \theta_{1,j} \leq \frac{2}{9},\ 0 < \theta_{2,j} \leq \frac{1}{9}$$

and the relation $-\phi_{1,j} - \phi_{2,j} + \theta_{0,j} + \theta_{1,j} + \theta_{2,j} = 1$ holds for keeping the requirement of volume balance.

3.3 Addition of Spilling-Water Condition of a Reservoir to Manifold Cell Model

Because a flash flood usually occurs in the typhoon-hitting period, spilling excess water from the storage reservoir is a necessary measure for safety considerations Spilling water is thus added as an additional inflow from upstream to downstream. Including the spilling-water condition of a reservoir in the manifold cell model is an important issues in model building.

The spilling-water condition can be added as an additional inflow to the streamflow part of the upper cell subsequently coming close to a reservoir as shown in **Fig. 6**, the equation of continuity for the manifold cell model then can be expressed as:

$$Q_{1,1}(t) + R(t) - Q_{2,1}(t) = \frac{dS_{2,1}(t)}{dt} \tag{29}$$

where, $R(t)$: spilling discharge to channel from a reservoir, cms.

Substituting $S_{2,1}(t) = M_1 Q_{2,1}(t)$ into eq. (29), where M_1 is storage constant, yields:

$$\frac{1}{k_a} S_{1,1}(t) + R(t) - \frac{1}{M_1} S_{2,1}(t) = \frac{dS_{2,1}(t)}{dt} \tag{30}$$

Integration of eq. (30) from t-1 to t by applying the trapezoidal rule yields:

$$\frac{1}{2k_a}(1+B)S_{1,1}(t) + (1+B)R(t) - \frac{1}{2M_1}(1+B)S_{2,1}(t) = (1-B)S_{2,1}(t) \tag{31}$$

or
$$\left[(1-B) + \frac{1}{2M_1}(1+B)\right] S_{2,1}(t) = \frac{1}{2k_a}(1+B)S_{1,1}(t) + \frac{1}{2}(1+B)R(t) \tag{32}$$

Substituting the relation of eq. (20) into eq. (32) and simplifying obtains:

$$\left[\left(1+\frac{1}{2M_1}\right) - \left(1-\frac{1}{2M_1}\right)B\right] S_{2,1}(t) = \frac{1}{2k_a}(1+B)\frac{\frac{1}{2}(1+B)I_j(t)}{\alpha_2 + \alpha_1 B} + \frac{1}{2}(1+B)R(t) \tag{33}$$

or
$$(\beta_2 + \beta_1 B)S_{2,1}(t) = \frac{1}{k_a}\frac{1+2B+B^2}{\alpha_2 + \alpha_1 B} I_j(t) + \frac{(1+B)(\alpha_2 + \alpha_1 B)}{2(\alpha_2 + \alpha_1 B)} R(t) \tag{34}$$

Rewriting eq. (34) into ARX form gives:

$$(\beta_2 + \beta_1 B)(\alpha_2 + \alpha_1 B)Q_{2,1}(t) = \frac{1}{4k_a M_1}(1+2B+B^2)I_j(t) + \frac{1}{2M_1}(\alpha_2 + \alpha_1 B + \alpha_2 B + \alpha_1 B^2)R(t) \tag{35}$$

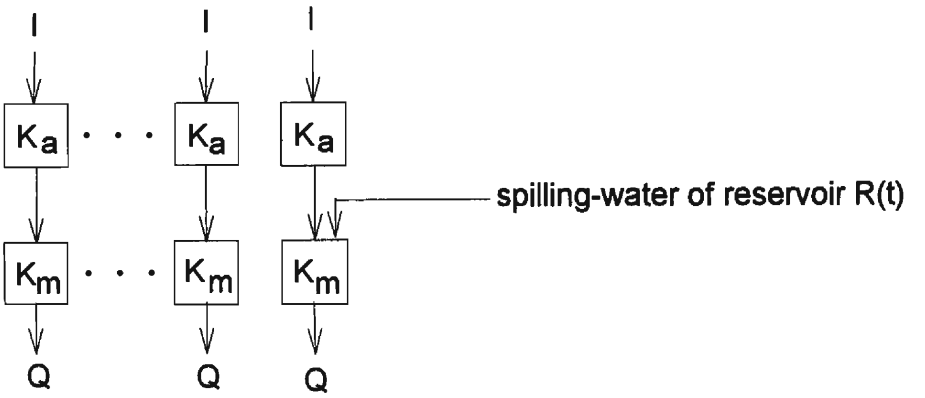

Fig. 6. Diagram of the manifold cell model including spilling-water condition.

$$\text{thus}\quad Q_{2,1}(t)=-\phi_{1,1}Q_{2,1}(t-1)-\phi_{2,1}Q_{2,1}(t-2)+\theta_{0,1}I_1(t)+\theta_{1,1}I_1(t-1)+\theta_{2,1}I_1(t-2)$$
$$+\phi_0R(t)+\phi_1R(t-1)+\phi_2R(t-2) \tag{36}$$

where,

$$\phi_{1,1}=-\frac{(2k_a-1)(2M_1+1)+(2k_a+1)(2M_1-1)}{(2k_a+1)(2M_1+1)},\quad \phi_{2,1}=\frac{(2k_a-1)(2M_1-1)}{(2k_a+1)(2M_1+1)}$$

$$\theta_{0,1}=\frac{1}{(2k_a+1)(2M_1+1)},\quad \theta_{1,1}=2\theta_{0,1},\quad \theta_{2,1}=\theta_{0,1}$$

and for $k_a\geq 1$, $M_1\geq 1$,

$$\phi_0=\frac{1}{(2M_1+1)}\leq\frac{1}{3},\quad \phi_1=\frac{2}{(2k_a+1)(2M_1+1)}\leq\frac{2}{9},\quad \phi_2=\frac{2k_a-1}{(2k_a+1)(2M_1+1)}\leq\frac{1}{9}$$

3.4 Introduction of the effect of time delay

Time delay is conceptually different from time lag. Time lag is defined as the average runoff time for a flood wave moving from initiation point to the outlet of a river basin. The concept of time lag can be illustrated by the conceptual model of linear reservoirs. On the other hand, time delay denotes the time interval from the start of rainfall to the time when runoff variation is significantly large. The concept of time delay can be explained by the conceptual model of linear channels. In a larger river basin, time delay will be longer. Consequently, the effect of time delay must be introduced into the manifold cell model.

Assuming that the time-delay effect is something related to the distance of cell to the outlet of a river basin, it can be expressed as:

$$D_j=D\cdot\frac{L_j}{L_{\max}}\quad\text{(hrs)} \tag{37}$$

in which, L_j : distance from the j^{th} cell to the outlet, km;

$L_{\max}$: total distance from the remotest upper cell to the outlet of a project

basin, km;
D : time delay, hrs.

4. Parameter Optimization of the Manifold Cell Model

Parameter calibration and verification are important procedures for the application of a hydrologic model. The purpose of calibration is an attempt to determine a set of adequate parameters in order that the resulting outcomes of the model will be as close as possible to those observed. The model with the calibrated parameters should be verified with several events that occur in the future or events remaining for verification. The simulated results of verified events should be within certain accuracy. That is, the residual errors between the simulation and the observed data are within a certain degree of acceptability.

The objective function for parameter optimization is set up in this study as:

$$OBJ=\left\{\frac{1}{m}\sum_{i=1}^{m}[Q_{obs}(i)-Q_{est}(i)]^2\cdot WT(i)\right\}^{\frac{1}{2}}+DQ \tag{38}$$

where, $WT(i)$: weighting constant of discharge at time i, $WT(i)=\dfrac{Q_{obs}(i)+\bar{Q}_{obs}}{2\bar{Q}_{obs}}$;
$Q_{obs}(i)$: observed discharge at time i, cms;
$\bar{Q}_{obs}$: mean of observed discharges;
$Q_{est}(i)$: estimated discharge at time i, cms;
m : duration of streamflow, hrs;
DQ : correction factor (14), if peak discharge of estimated streamflow $(Q_p)_{est}$ is larger than peak discharge of observed streamflow, $(Q_p)_{obs}$, $DQ=0$; if $(Q_p)_{est}<(Q_p)_{obs}$, then $DQ=[(Q_p)_{obs}-(Q_p)_{est}]/m^2$.

If the model has a superior accuracy, OBJ will be close to zero.

The method of steepest descent is chosen for parameter optimization in this study. The principle of the steepest descent in parameter optimization (5, 15) can be briefly described as:

Let $f(X)$ be the objective function as shown in eq. (38), X is a parameter vector of the model. Assuming that $f(X)$ is a differentiable function of the first order, and for any initial value X^0, a neighboring point X^0+dX can be found to satisfy $f(X^0+dX)<f(X^0)$ and to meet the requirement of $df=f(X^0)-f(X^0+dX)=$maximum.

Let us define $(ds)^2=\sum_{i=1}^{m}(dX_i)^2$

or $$1-\sum_{i=1}^{m}\left(\frac{dX_i}{ds}\right)^2=0 \tag{39}$$

where, $\dfrac{dX_i}{ds}$: cosine of direction, and

$$\frac{df}{ds}=\sum_{i=1}^{m}\frac{\partial f}{\partial X_i}\frac{dX_i}{ds} \tag{40}$$

The so-called steepest descent method is to properly choose $\dfrac{dX_i}{ds}$ so that the

maximum value of $\frac{df}{ds}$ can be found out.

When the lagrange multiplier is applied to eq. (39), we have

$$L\left(\frac{dX_i}{ds}\right)=\sum_{i=1}^{m}\frac{\partial f}{\partial X_i}\frac{dX_i}{ds}+\lambda\left[1-\sum_{i=1}^{m}\left(\frac{dX_i}{ds}\right)^2\right] \tag{41}$$

If there is a set of solutions of $\frac{dX_i}{ds}$ $(i=1,2,\cdots,m)$ in eq. (41), the following two equations should be satisfied.

$$\nabla_{\frac{dX_i}{ds}}L=\frac{\partial f}{\partial X_i}-2\lambda\frac{dX_i}{ds}=0 \qquad (i=1,2,\cdots\cdots,m) \tag{42}$$

and $$\nabla_\lambda L=1-\sum_{i=1}^{m}\left(\frac{dX_i}{ds}\right)^2=0 \tag{43}$$

Solving eqs. (42) and (43), we get:

$$\frac{dX_i}{ds}=\frac{1}{2\lambda}\frac{\partial f}{\partial X_i} \tag{44}$$

and $$\lambda=\pm\frac{1}{2}\left[\Sigma\left(\frac{\partial f}{\partial X_i}\right)^2\right]^{\frac{1}{2}} \tag{45}$$

Substituting eq. (45) into eq. (44) yields:

$$\frac{dX_i}{ds}=\frac{\pm\frac{\partial f}{\partial X_i}}{\left[\sum_{i=1}^{m}\left(\frac{\partial f}{\partial X_i}\right)^2\right]^{1/2}} \tag{46}$$

or $$dX_i=\frac{\pm ds}{\left[\sum_{i=1}^{m}\left(\frac{\partial f}{\partial X_i}\right)^2\right]^{1/2}}\frac{\partial f}{\partial X_i} \tag{47}$$

Let $g_k=\frac{\partial f}{\partial X_k^i}$, $\alpha=\frac{\pm ds}{\left[\sum_{i=1}^{m}\left(\frac{\partial f}{\partial X_i}\right)^2\right]^{1/2}}=\frac{\mathrm{ds}}{2\lambda}$

and $X_i^{k+1}-X_i^k=dX_i^k$

where, k: number of iteration.

thus $$X_i^{k+1}=X_i^k+\alpha_k g_k \tag{48}$$

In eq. (48), α_k is called the step size. If a smaller α_k is chosen, the speed of convergence is rather slow. On the contrary, an up-and-down fluctuation could probably occur near the optimal value if too large an α_k value was chosen. An appropriate quadratic form of curvature is adopted in this study to increase its efficiency of convergence as shown below:

Let $$f(X^1)=f(X^0+\alpha_0 g_0)\approx a\alpha^2+b\alpha+c=\Pi(\alpha) \tag{49}$$

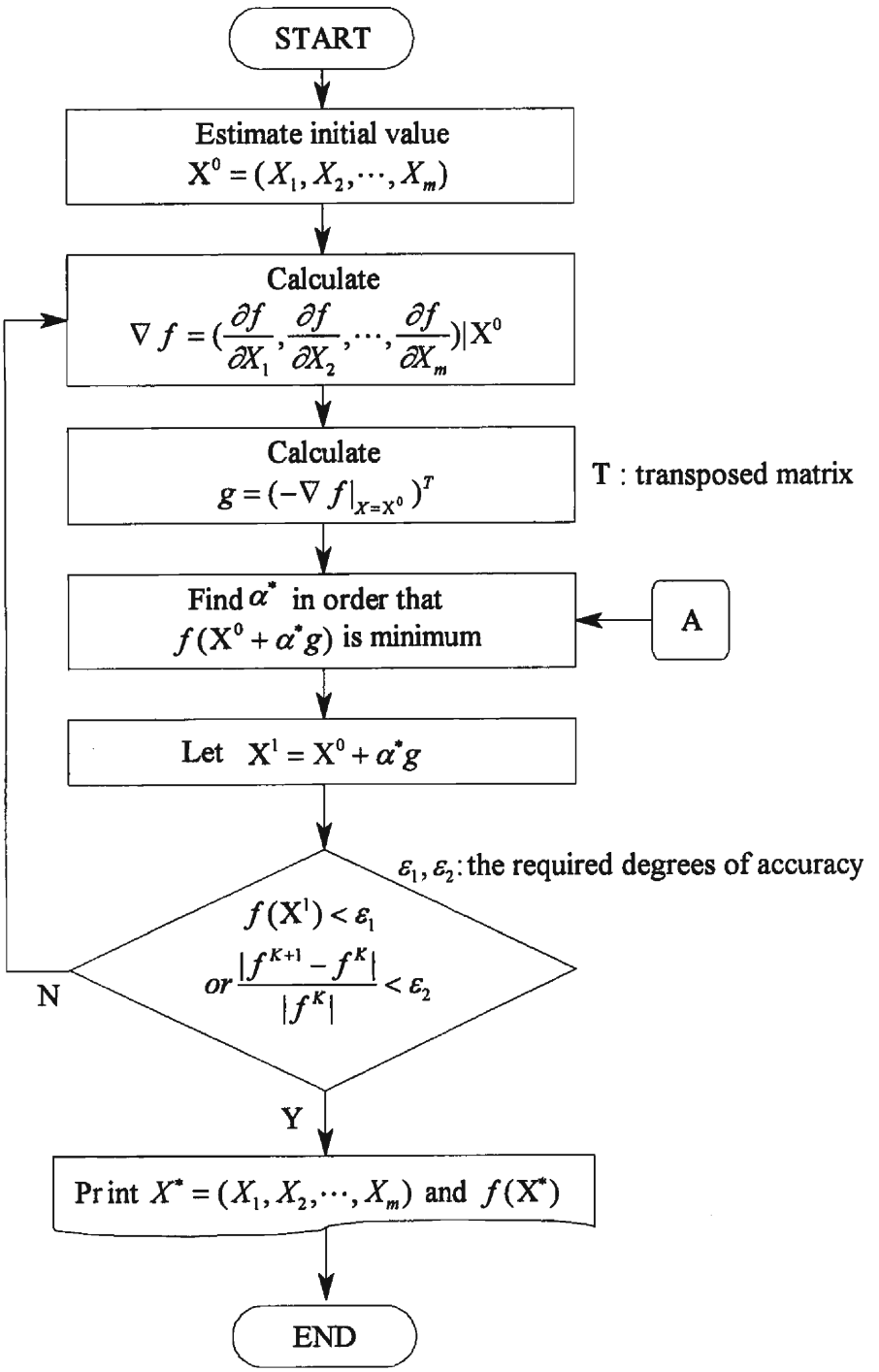

Fig. 7. Flow chart of the steepest descent method.

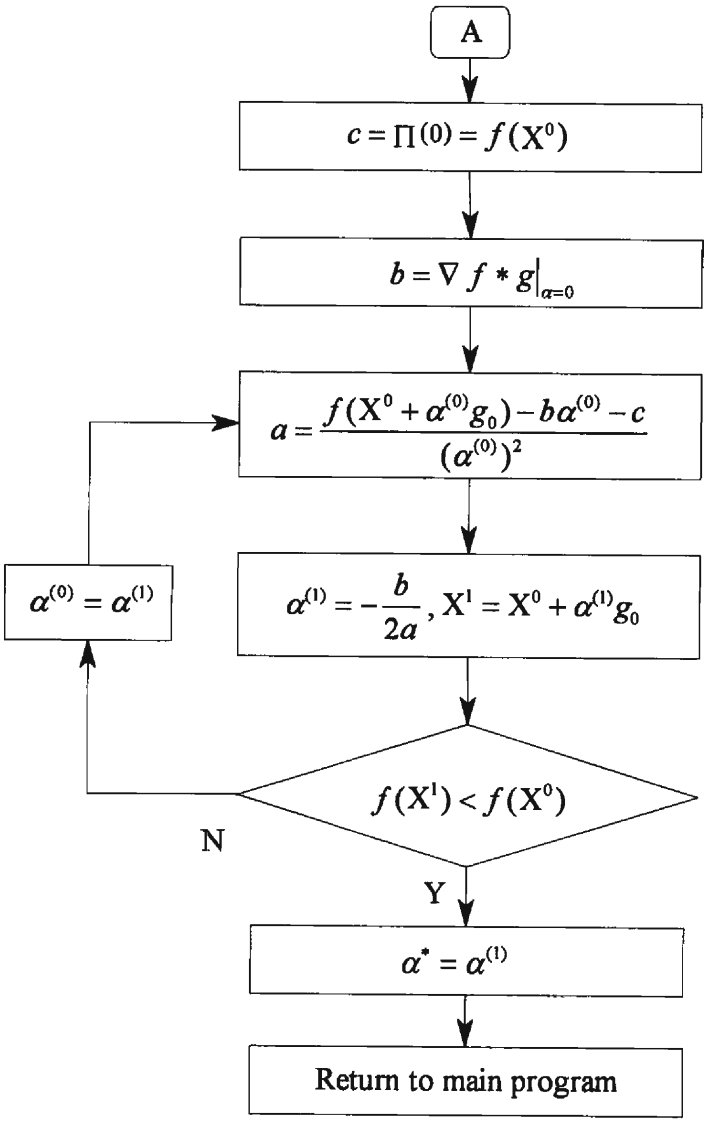

Fig. 8. Flow chart for determining the optimal step size of the steepest descent method.

where $c = \Pi(0) = f(X^0)$ (50)

$$b = \frac{\partial \Pi}{\partial \alpha}\bigg|_{\alpha=0} = \frac{\partial f}{\partial \alpha}\bigg|_{\alpha=0}$$

$$\because \frac{\partial f}{\partial \alpha} = \frac{\partial f}{\partial X} \cdot \frac{\partial X}{\partial \alpha} = \nabla f \cdot g$$

$$\therefore b = \nabla f \cdot g|_{\alpha=0} \tag{51}$$

For any value of $\alpha^{(0)}$

$$f(X^1)=f(X^0+\alpha^{(0)}g_0)\approx\alpha(\alpha^{(0)})^2+b(\alpha^{(0)})+c$$

$$\therefore a=\frac{f(X^1)-b(\alpha^{(0)})-c}{(\alpha^{(0)})^2} \tag{52}$$

Let $\Pi(\alpha)$ be the minimum, i.e., $\frac{\partial\Pi(\alpha)}{\partial\alpha}=0$ for finding out the optimal step size α^* as:

$$\underset{\alpha}{\text{Min}}\,\Pi(\alpha)=\underset{\alpha}{\text{Min}}\,(a\alpha^2+b\alpha+c) \tag{53}$$

so $$\frac{\partial\Pi}{\partial\alpha}=2a\alpha+b=0$$

$$\therefore\alpha^{(1)}=-\frac{b}{2a}\text{ and }\alpha^{(1)}<\alpha^{(0)} \tag{54}$$

Let $X^1=X^0+\alpha^{(1)}g_0$. If $f(X^{-1})<f(X^0)$, then $\alpha^{(1)}$ is equal to the optimal step size α^*; otherwise, let $\alpha^{(0)}=\alpha^{(1)}$. Repeat the procedure until α^* can be determined. **Figs. 7** and **8** show the flow charts of the method of steepest descent for parameter optimization.

5. Real-time Prediction of Model

For extending the applicability of hydrologic prediction, Kalman filter is combined with the manifold cell model in this study. Kalman filter is a recursive process which is a very powerful tool for the prediction by hydrologic model (1, 14).

Equation of state and euation of observation are two essential governing equations which should be considered.

Equation of State: $X(t+1)=\phi(t)X(t)+W(t)$ (55)

where, $X(t)$: state vector of system at time t;
$\phi(t)$: transformed coefficient matrix at time t;
$W(t)$: state error vector at time t.

Equation of Observation: $Y(t)=H(t)X(t)+V(t)$ (56)

where, $Y(t)$: observation vector at time t;
$H(t)$: coefficient matrix at time t;
$V(t)$: observation error vector at time t.

Assuming that state error of system $W(t)$ and observation error $V(t)$ follow Gauss distribution, $E[W(t)]=0$ and $E[V(t)]=0$ can be achieved. The optimal state for next time stage $t+1$, $\hat{X}(t+1\,|\,t)$ and the optimal predicting value for next time stage, $\hat{Y}(t+1\,|\,t)$ can be expressed respectively as:

$$\hat{X}(t+1\,|\,t)=\hat{X}(t\,|\,t) \tag{57}$$

$$\hat{Y}(t+1\,|\,t)=\mathrm{H}(t+1)\hat{X}(t+1\,|\,t) \tag{58}$$

where, $(t+1\,|\,t)$: given data at time t, the finded predicting value for time $t+1$. "Predicting" is called for the process.

$(t|t)$: given data at time t, the finded predicting value for time t as "filtering".

As derivation of modified formulation of the manifold cell model as eq. (28), every cell can be assumed as a linear structure. The resulting total streamflow at the outlet of a river basin can be expressed as:

$$Q(t)=\sum_{j=1}^{n} Q_j(t)$$

$$=\sum_{j=1}^{n}\{-\phi_{1,j}Q_j(t-1)-\phi_{2,j}Q_j(t-2)$$

$$+\theta_{0,j}I_j(t-D_j)+\theta_{1,j}I_j(t-1-D_j)+\theta_{2,j}I_j(t-2-D_j)\}+V(t) \tag{59}$$

where, n : total number of subareas in the river basin;

D : time delay of j^{th} cell, hrs;

$V(t)$: observation error;

$I(t)$: rainfall to j^{th} cell at time t, cms;

$Q_j(t)$: outflow discharge of j^{th} cell at time t, cms;

$Q(t)$: outflow discharge of total river basin, cms;

$\phi_{1,j},\phi_{2,j},\theta_{0,j},\theta_{1,j},\theta_{2,j}$: coefficients.

Eq.(59) can be expressed as the form of state space as:

$$Q(t)=H(t)X(t)+V(t) \tag{60}$$

where, $H(t)=[Q_1(t-1),Q_1(t-2),\cdots\cdots,Q_n(t-1),Q_n(t-2),$

$$I_1(t-D_1),I_1(t-D_1-1),I_1(t-D_1-2),\cdots\cdots,$$

$$I_n(t-D_n),I_n(t-D_n-1),I_n(t-D_n-2)] \tag{61}$$

and $X(t)=[-\phi_{1,1},-\phi_{2,1},\cdots\cdots,-\phi_{1,n},-\phi_{2,n},\theta_{0,1},\theta_{1,1},\theta_{2,1},\cdots\cdots,\theta_{0,n},\theta_{1,n},\theta_{2,n}]^T$ (62)

Kalman filter can be combined with the manifold cell model for flood prediction by eq. (60).

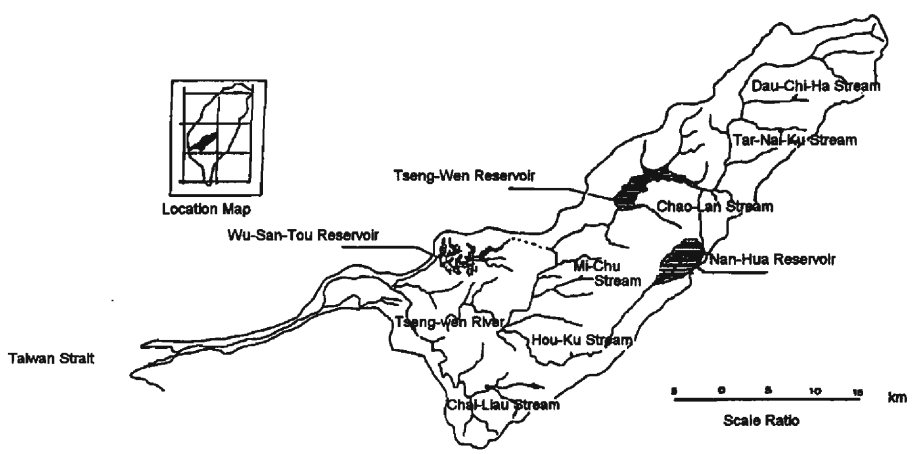

Fig. 9. Location and layout of Tseng-Wen River basin, Taiwan.

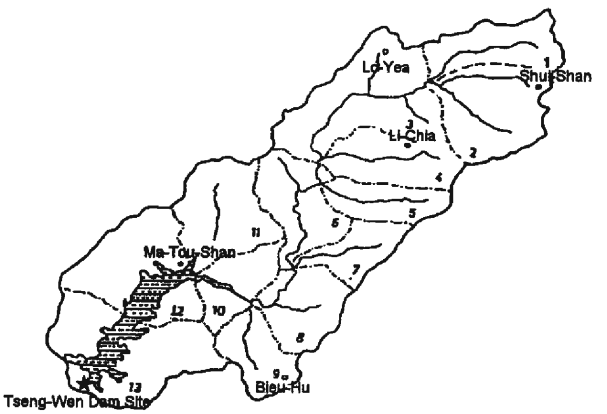

Fig. 10. Flow network of cells for the upstream reservoir watershed of Tseng-Wen River Basin.

6. Practical Applications

For verification of the applicability of the manifold cell model, Tseng-wen River Basin, Taiwan was adopted as a project basin.

6.1 Brief Introduction of the Project Basin

Tseng-wen River Basin is located at the southwestern part of Taiwan as shown in **Fig. 9**. Its watershed area is 1,177 km^2, the length of the main steam is 138.5 km and the mean gradient of the river is from 1/1000 to 1.5/1000 flowing westward to the Taiwan Strait. Three reservoirs, namely, Wu-shan-tou, Tseng-wen and Nan-hua were built in the project basin. It is regarded as a comprehensive reservoir watershed and the most prosperous area in southwestern Taiwan.

6.2 Analysis of Hydrologic Records and Physiographic Data

6.2.1 Zoning of Project Basin

For ease of analyzing the manifold cell model in the project basin, classification of a

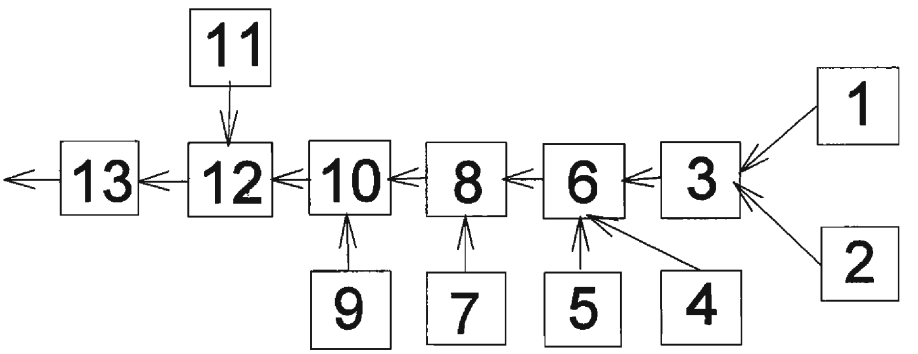

Fig. 11. Block diagram of zoning of cells in the upstream reservoir watershed of Tseng-Wen River Basin.

Fig. 12. Flow network of cells in the downstream plain watershed of Tseng-Wen River Basin.

cell was ascertained directly from the topography maps. Each cell was determined by the orientation of river pattern and divide form which could be regarded as an independent hydrologic element for analysis. For simplification, Tseng-wen River Basin is divided into two zones; namely, the upstream reservoir watershed and the downstream plain watershed. In the upstream watershed, five raingage stations, namely, Ma-tou-shan, Lo-yea, Shui-shan, Li-chia, Bieu-hu and one stage gaging station at Tseng-wen Dam Site were set up. In the downstream plain watershed, three raingage stations, namely, Tseng-wen New Village, Shi-a-li-kuan, Nan-hua and one gaging station at Ma-shan Bridge were built.

The flow network of cells of the upstream reservoir watershed is shown in **Fig. 10**, and block diagram of connected subareas connecting from upstream to downstream in the upstream reservoir watershed is drawn in **Fig. 11**. Flow network of cells and block diagram of subareas for the downstream plain watershed are shown in **Figs. 12** and **13**. Physiographic characteristics of cell including area of cell, length of river courses, distance to outlet, connecting cell of upstream, etc., for the upstream reservoir

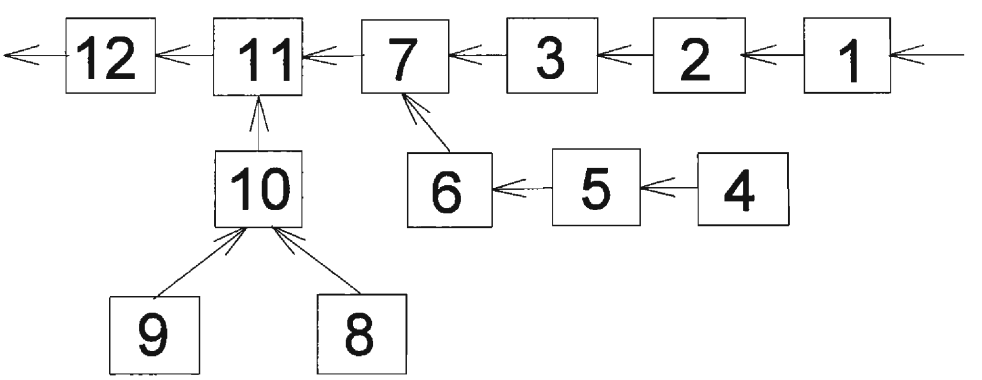

Fig. 13. Block digram of zoning of cells in the downstream plain watershed of Tseng-Wen River Basin.

Table 2. Physiographic characteristics of cells in Tseng-Wen River Basin, Taiwan

(A) Upstream reservoir watershed

number of cells	area (km^2)	length of main stream (km)	distance to outlet (km)	sequence number of upstream cell
1	53.5	8.72	54.84	---
2	52.0	9.73	49.05	1
3	38.1	6.85	40.78	2
4	52.3	11.08	82.74	---
5	66.4	20.56	66.92	4
6	47.5	19.31	46.99	5
7	62.5	19.40	27.63	3,6
8	54.5	13.08	52.16	---
9	31.8	13.62	45.89	---
10	45.1	21.15	28.51	8,9
11	46.3	8.32	13.77	7,10
12	58.0	9.61	4.81	11

(B) Downstream plain watershed

number of cells	area (km^2)	length of main stream (km)	distance to outlet (km)	sequence number of upstream cell
1	29.1	10.87	49.31	---
2	45.2	8.89	48.32	---
3	62.6	12.48	37.64	1,2
4	34.4	8.99	35.91	---
5	22.1	8.36	35.60	---
6	37.8	9.14	26.84	3,4,5
7	20.4	8.98	26.78	---
8	31.1	5.67	19.44	6,7
9	25.0	8.72	20.96	---
10	25.5	5.15	14.03	8,9
11	41.6	11.13	17.02	---
12	52.1	5.31	8.80	11,10
13	55.9	6.14	3.07	12

watershed and downstream plain watershed are summarized in **Table 2**.

6.2.2 Determination of Areal Average Rainfall and Effective Rainfall

For determining the areal average rainfall in the project area, Thiessen's polygon method was adopted and a polygon network controlled by raingage stations is drawn as **Fig. 14**. **Table 3**(A) and 3(B) show the control area and weighting for each raingage station of the upstream reservoir watershed and downstream plain watershed, respectively. Due to the lack of detailed infiltration data in the project area, Φ—index was adopted for estimating the effective rainfall of ordinary situation (11). During the spilling-water situation of typhoon-hitting period in the project basin, $\Phi = 5$ mm/hr is usually used in Taiwan.

6.2.3 Selection of Storm and Flood Records

Typhoon events occurring from 1976 to 1986 were collected as calibration and verification of the manifold cell model for event simulation as shown in **Table 4**, in

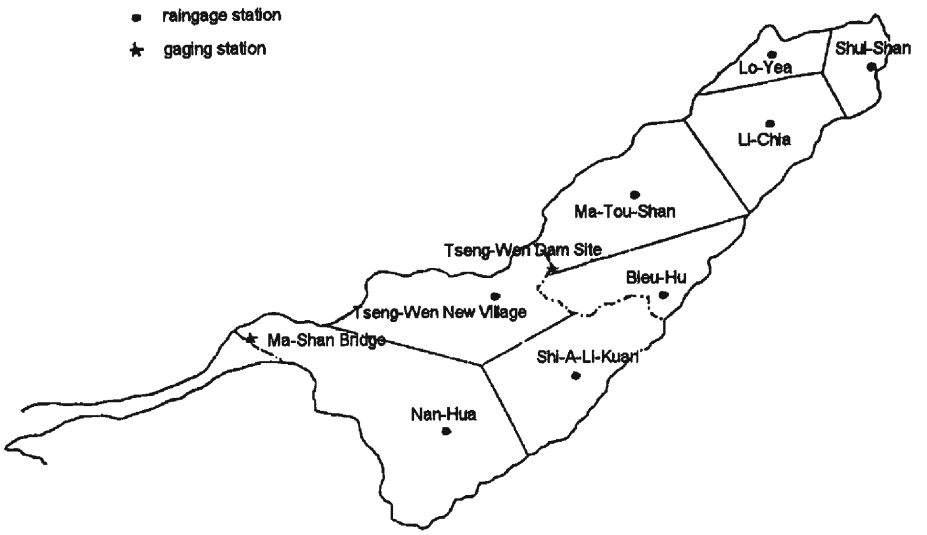

Fig. 14. Thiessen's polygons network for raingage stations in Tseng-Wen River Basin.

which five typhoon events for upstream reservoir watershed and five typhoon events for downstream plain watershed are included. During hitting of Typhoon Billie on August 10, 1976, spilling flood from spillways of Tseng-wen Reservoir occurred at a peak discharge of 900 cms, which made the analysis of the manifold cell model more complicated.

6.3 Criteria of Evaluation for the Accuracy of Manifold Cell Model

For checking the suitability of the manifold cell model to flood estimation of the project basin, the following four criteria of evaluation were adopted:

Table 3. Control areas and weightings of raingage station divided by Thiessen's polygon network in Tseng-Wen River Basin

(A) Upstream reservoir watershed

station name	Ma-Lou-Shan	Lo-Yea	Shui-Shan	Li-Chia	Bieu-Hu
control area (km^2)	181.4	42.4	44.3	128.7	84.3
weighting	0.38	0.09	0.09	0.27	0.17

(B) Downstream plain watershed

station name	Tseng-Wen New Village	Shi-A-Li-Kuan	Nan-Hua
control area (km^2)	110.3	122.7	367.3
weighting	0.18	0.20	0.62

Table 4. List of typhoon events occurring in Tseng-Wen River Basin, Taiwan

region	typhoon name	time of occurrence	duration of stream flow (hrs)	Φ-index (mm/hr)
upstream reservoir watershed	* Billie	1976.08.10	98	5.0
	Amy	1977.08.22	54	4.8
	Vera	1980.08.31	48	5.2
	Alex	1984.07.03	75	8.3
	Abby	1986.09.19	93	7.5
downstream plain watershed	* Billie	1976.08.10	104	2.8
	Irving	1979.08.14	155	2.2
	Norris	1980.08.27	96	3.5
	Alex	1984.07.03	42	3.8
	Abby	1986.09.19	80	2.6

* spilling water from Tseng-Wen Reservoir.

(1) Coefficient of Efficiency, CE

$$CE=1-\frac{\sum_{i=1}^{n}[Q_{obs}(i)-Q_{est}(t)]^2}{\sum_{i=1}^{n}[Q_{obs}(i)-\bar{Q}_{obs}]^2} \tag{63}$$

in which, $Q_{est}(t)$: estimated discharges by the cell model, cms;
$Q_{obs}(t)$: observed discharges, cms;
$\bar{Q}_{obs}$: mean of observed discharges, cms;
n : number of records.

If CE is near to 1, it means that there is a superior conformity between the estimated and the observed. The larger CE is, the more accurate the model becomes.

(2) Error of Peak Discharge, $EQ_p(\%)$

$$EQ_p=\frac{(Q_p)_{est}-(Q_p)_{obs}}{(Q_p)_{obs}}\times 100\% \tag{64}$$

where, $(Q_p)_{est}$: estimated peak discharge, cms;
$(Q_p)_{obs}$: observed peak discharge, cms;

If the estimated peak discharge is larger than the observed peak discharge, a positive EQ_p is obtained, and vice versa. The smaller EQ_p is, the more accurate the model. is.

(3) Error of Time to Peak Discharge, ET_p (hours)

$$ET_p=(T_p)_{est}-(T_p)_{obs} \tag{65}$$

where, $(T_p)_{est}$: estimated time to peak discharge, hrs;
$(T_p)_{obs}$: observed time to peak discharge, hrs;

If the model has a good accuracy in error of time to peak discharge, then ET_p approaches zero.

(4) Value of Objective Function, OBJ

For evaluating the accuracy of the manifold cell model adopted, value of objective function in eq. (38) was also adopted in this study.

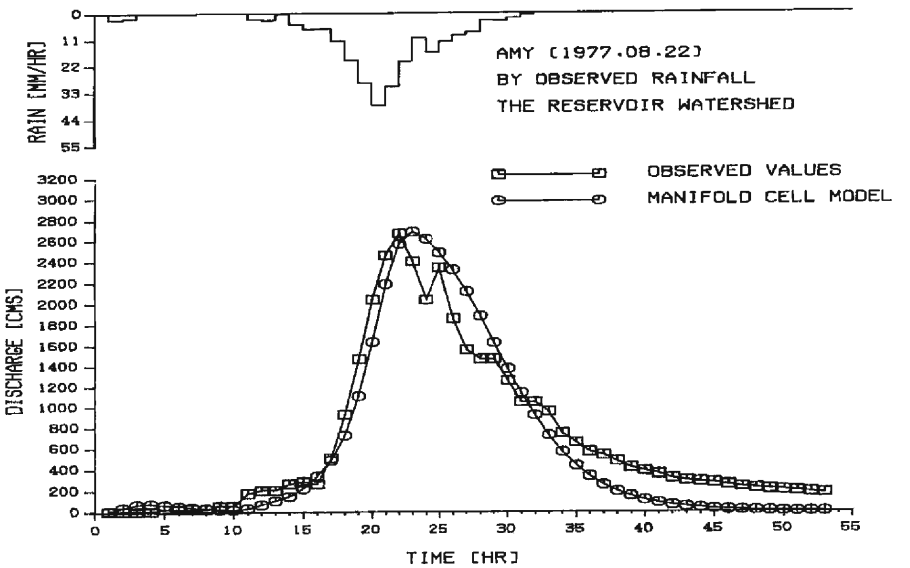

Fig. 15. Simulated results vs. the observed values in the upstream reservoir watershed of Tseng-Wen River Basin (Typhoon Amy, 1977).

6.4 Discussion of Results

(1) The simulated results of historical typhoon events for the upstream reservoir watershed of Tseng-wen River Basin by applying the manifold cell model are shown in **Table 5**(A) and two examples are illustrated in **Figs. 15–16**.

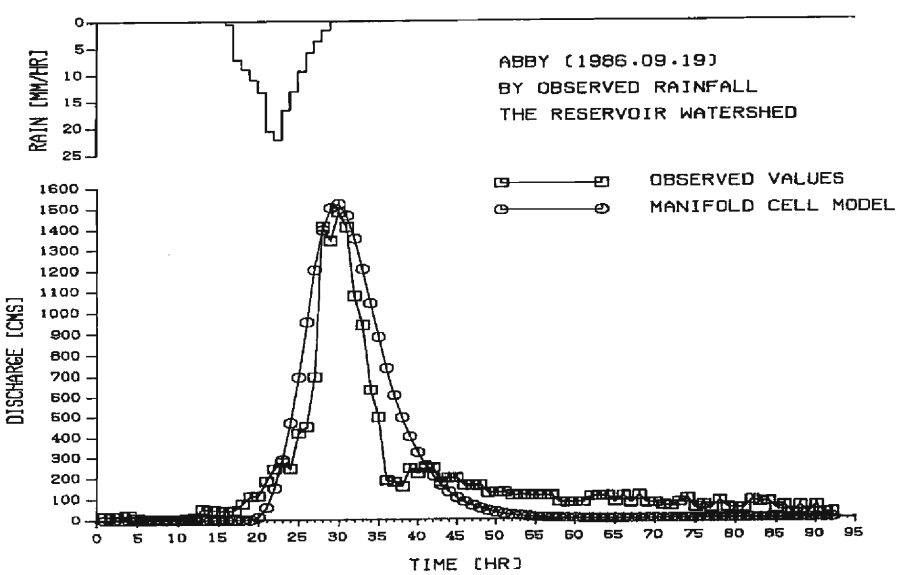

Fig. 16. Simulated results vs. the observed values in the upstream reservoir watershed of Tseng-Wen River Basin (Typhoon Abby, 1986).

Table 5. Results of verification for the manifold cell model

(A) Upstream reservoir watershed

item	typhoon name	Billie 1976.08.10	Amy 1977.08.22	Vera 1980.08.31	Alex 1984.07.03	Abby 1986.09.19
observed values	Qp	2808	2660	1682	4361	1481
	Tp	16	22	26	10	30
manifold cell model	Qp	2841	2686	1568	4366	1433
	Tp	17	23	28	10	28
	CE	0.78	0.90	0.66	0.65	0.68
	EQp (%)	1.18	0.98	-6.78	0.15	-3.24
	ETp (hrs)	1	1	2	0	-2
	OBJ	0.0138	0.0276	0.0213	0.0397	0.0356

(B) Downstream plain watershed

item	typhoon name	Billie 1976.08.10	Irving 1979.08.14	Norris 1980.08.27	Alex 1984.07.03	Abby 1986.09.19
observed values	Qp	1824	1490	1182	1358	805
	Tp	20	15	16	15	18
manifold cell model	Qp	1905	1487	1180	1280	779
	Tp	21	13	17	15	17
	CE	0.96	0.81	0.78	0.91	0.94
	EQp (%)	4.45	-0.20	-0.17	5.74	-3.23
	ETp (hrs)	1	-2	1	0	-1
	OBJ	0.0118	0.0279	0.0149	0.0197	0.0265

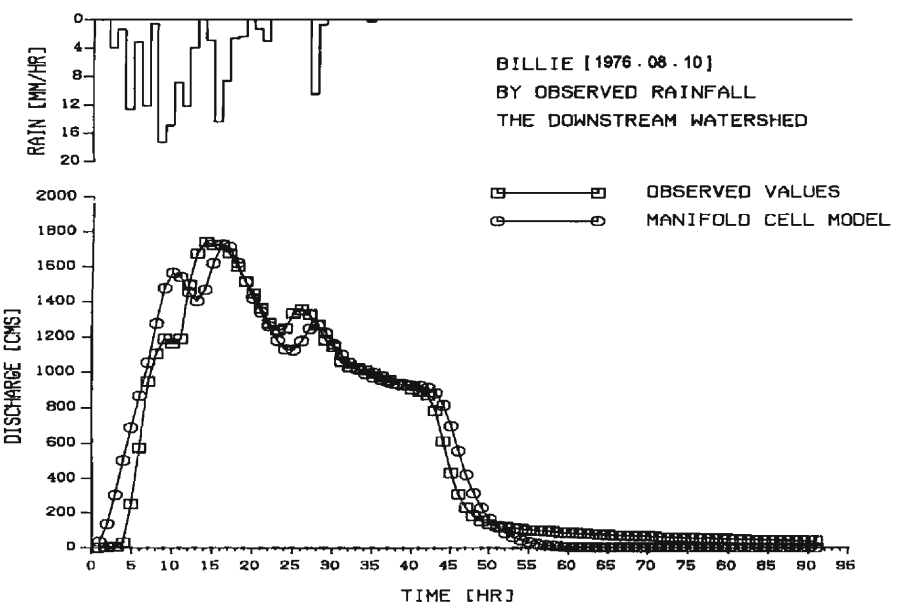

Fig. 17. Simulated results vs. the observed values in the downstream plain watershed of Tseng-Wen River Basin (Typhoon Billie, 1976).

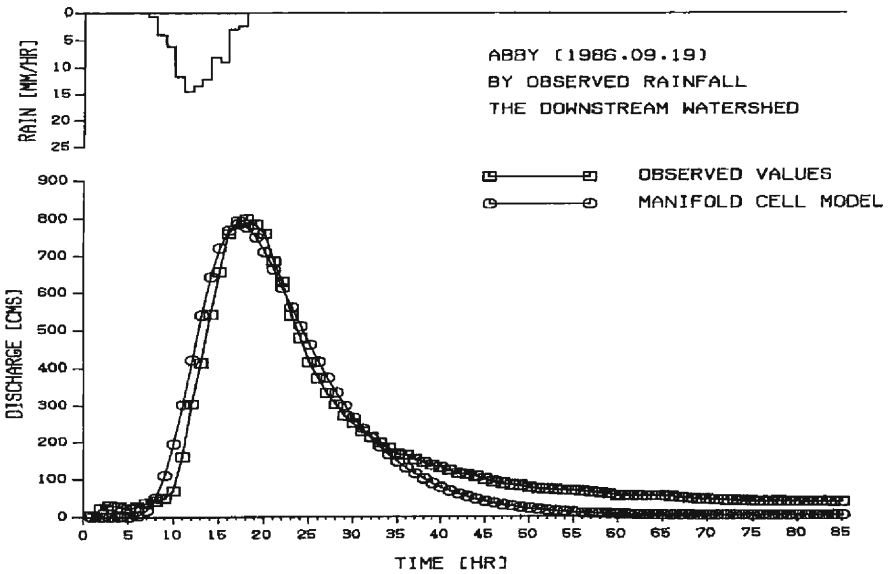

Fig. 18. Simulated results vs. the observed values in the downstream plain watershed of Tseng-Wen River Basin (Typhoon Abby, 1986).

A. *CE* of Typhoon Alex is the minimum, ($CE=0.65$), and that of Typhoon Amy is the maximum ($CE=0.90$).

B. Errors of peak discharge were within 7%.

C. Errors of time to peak discharge were within 2 hours.

D. The maximum *OBJ* was found in Typhoon Alex ($OBJ=0.0397$), next was Typhoon Abby ($OBJ=0.0356$), and the rest were less than 0.03.

Table 6. Optimized parameters of the manifold cell model in Tseng-Wen River Basin, Taiwan

(A) Upstream reservoir watershed

typhoon name	*Ka* (hrs)	*M* (hrs)	*Dj* (hrs)
Billie	3.34	1.50	0
Amy	2.82	1.63	0
Vera	2.11	1.00	0
Alex	1.45	1.01	0
Abby	2.68	1.36	0
Average	2.48	1.30	0

(B) Downstream plain watershed

typhoon name	*Ka* (hrs)	*M* (hrs)	*Dj* (hrs)
Billie	4.63	2.20	8
Irving	1.78	1.02	14
Norris	3.00	1.50	14
Alex	3.30	1.59	14
Abby	3.58	2.16	11
Average	3.26	1.69	12.2

(2) The results for the downstream plain watershed are shown in **Table 5**(B) and two examples are illustrated in **Figs. 17–18**.

A. The minimum CE=Typhoon Norris (CE=0.78), the maximum CE=Typhoon Billie (CE=0.96).

B. Errors of peak discharge were less than 5.74%.

C. Errors of time to peak discharge were −2 hours for Typhoon Irving, and less than 1 hour for the rest.

D. The maximum objective function was found in Typhoon Irving (OBJ=0.0279), and the minimum OBJ in Typhoon Billie (OBJ=0.0118).

(3) Spilling water condition from spillways of a reservoir during typhoon-hitting period can be included in the manifold cell model. Taking the case study of Typhoon Billie for example, the simulated hydrographs and results are shown in **Fig. 17** and **Table 5**(B). It can be seen from **Fig. 17** that the manifold cell model well simulates the effect of spilling water to the downstream of the reservoir. The coefficient of efficiency of the simulated results for the manifold cell model is of satisfactory accuracy with CE above 0.95.

(4) In general, the simulated results in the downstream plain watershed are much better than those obtained in the upstream reservoir watershed. The reasons are probably due to the effect of rugged topography on hydrologic phenomena causing uneven distribution of rainfall in the upstream reservoir watershed.

(5) Parameters adopted in the manifold cell model were obtained by applying the method of the steepest descent as shown in **Tables 6**(A) and **6**(B) for both upstream

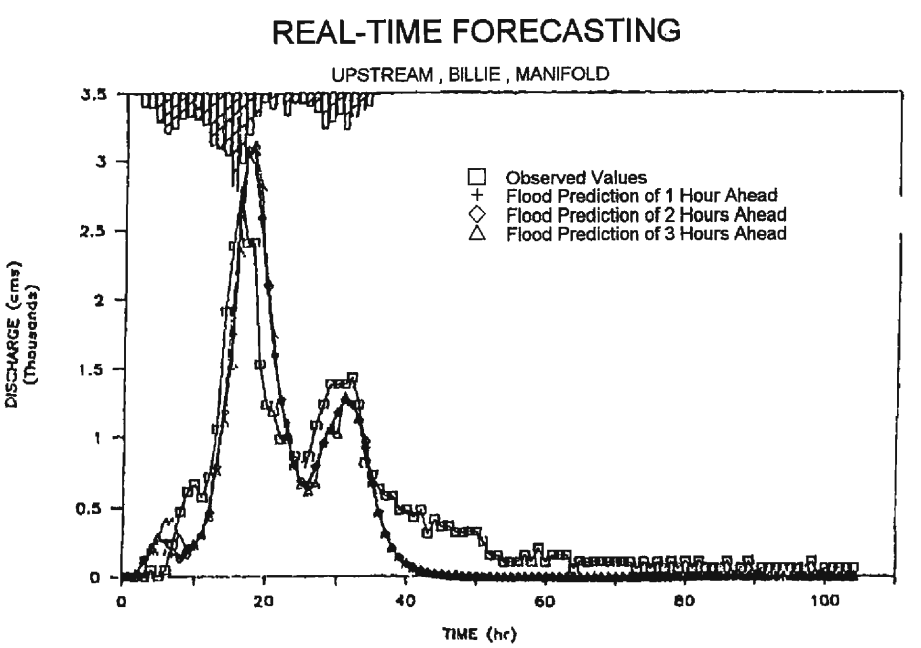

Fig. 19. Flood predictions of 1, 2 and 3 hours ahead for Typhoon Billie (1976) in the upstream reservoir watershed of Tseng-Wen River Basin.

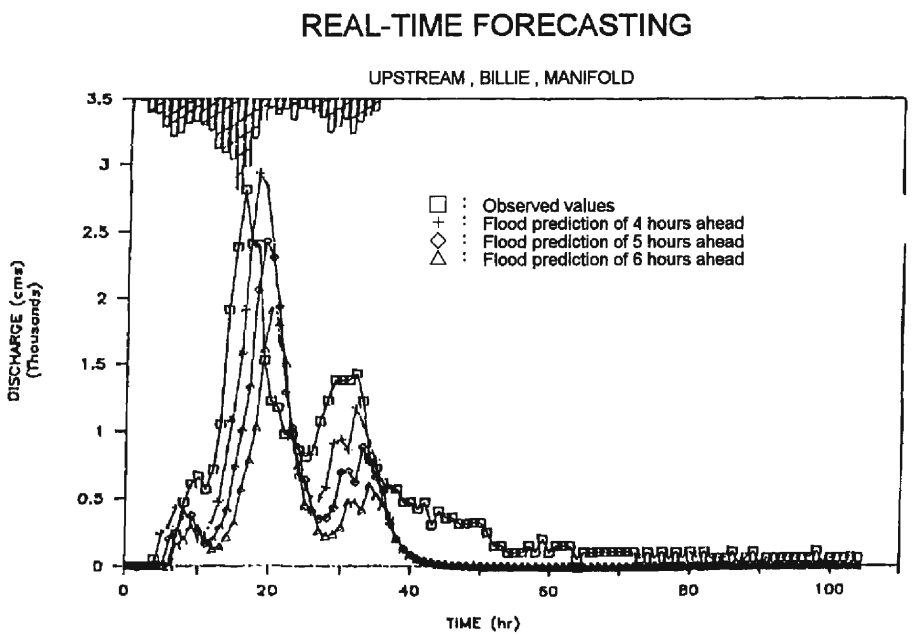

Fig. 20. Flood predictions of 4, 5 and 6 hours ahead for Typhoon Billie (1976) in the upstream reservoir watershed of Tseng-Wen River Basin.

reservoir watershed and downstream plain watershed. Values of those parameters obtained by the method of parameter optimization may be used as the basis for applying to the flood estimation in the project basin.

(6) The manifold cell model was combined with Kalman filter in this study for applying to flood prediction of one to six hours ahead in the project basin. Examples of flood prediction of 1, 2, 3, 4, 5 and 6 hours ahead for Typhoon Billie of the upstream reservoir watershed are shown in **Figs. 19** to **20** and **Table 7**. Examples for flood prediction of 1～6 hours ahead for Typhoon Andy of the downstream plain watershed are shown in **Figs. 21** to **22** and **Table 8**. From the predicted results shown, flood predictions of 1～3 hours are still satisfactory. The larger the lead time for prediction is, the poorer the accuracy of the model becomes. How to predict most accurately the trend of a

Table 7. Results of flood prediction from 1 to 6 hours ahead for Typhoon Billie (1976) in the upstream reservoir watershed of Tseng-Wen River Basin, Taiwan

time of prediction	predicted values					
	Qp(cms)	Tp(hr)	CE	EQp(%)	ETp	OBJ
1-hr ahead	3074	17	0.82	9.55	1	0.0310
2-hr ahead	3075	17	0.79	9.60	1	0.0336
3-hr ahead	3119	18	0.75	11.16	2	0.0380
4-hr ahead	2933	18	0.65	4.53	2	0.0475
5-hr ahead	2431	19	0.45	-13.37	3	0.0971
6-hr ahead	1905	20	0.21	-32.10	4	0.1608
observed values	2806	16	---	---	---	---

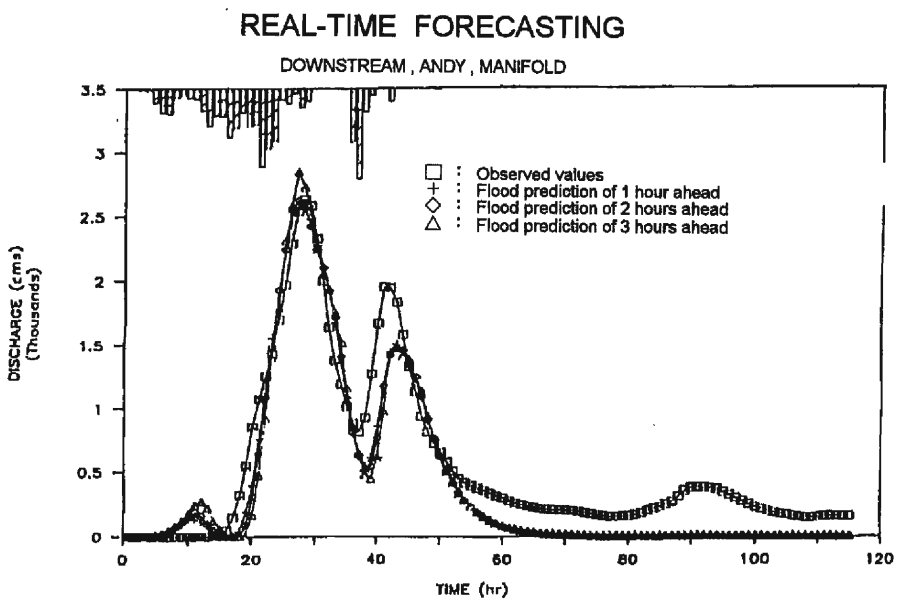

Fig. 21. Flood predictions of 1, 2 and 3 hours ahead for Typhoon Andy (1982) in the downstream plain watershed of Tseng-Wen River Basin.

storm/flood as early as possible during the typhoon-hitting period is one of the important issues in disaster prevention research. It can be seen that the manifold cell model is the appropriate hydrologic model for applying to flood prediction in the project

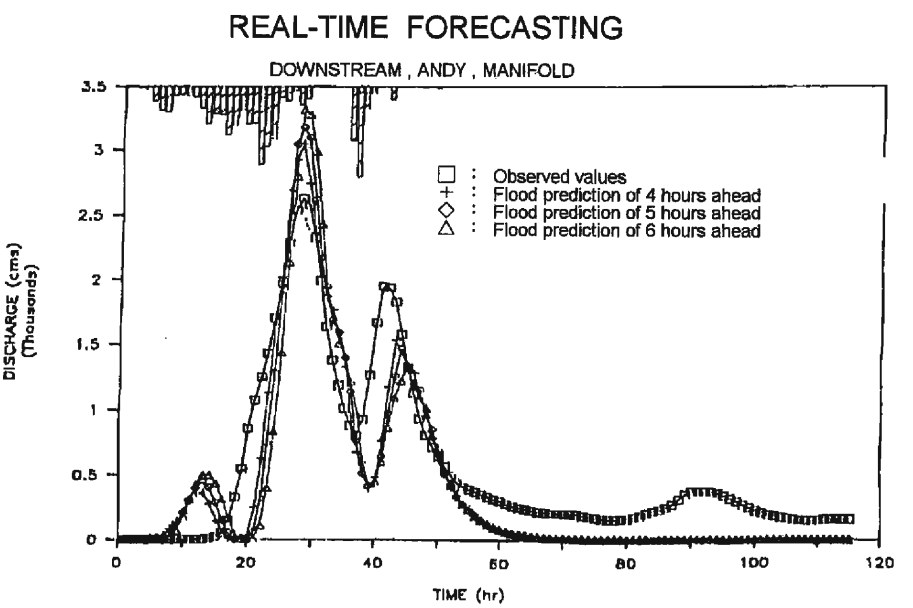

Fig. 22. Flood predictions of 4, 5 and 6 hours ahead for Typhoon Andy (1982) in the downstream plain watershed of Tseng-Wen River Basin.

Table 8. Results of flood prediction from 1 to 6 hours ahead for Typhoon Andy (1982) in the downstream plain watershed of Tseng-Wen River Basin, Taiwan

time of prediction	predicted values					
	Qp(cms)	Tp(hr)	CE	EQp(%)	ETp	OBJ
1-hr ahead	2558	27	0.87	-2.75	-1	0.0257
2-hr ahead	2623	27	0.85	-0.28	-1	0.0224
3-hr ahead	2848	27	0.82	8.29	-1	0.0249
4-hr ahead	3049	28	0.77	15.95	0	0.0291
5-hr ahead	3180	28	0.71	20.92	0	0.0338
6-hr ahead	3321	28	0.63	26.29	0	0.0386
observed values	2630	28	---	---	---	---

river basin.

(7) The effect of time delay when applying the manifold cell model is that longer the distance from the project site to the outlet, the more significant the effect of time delay becomes. The longer the time delay D_j will dampen the effect of uncertainty of hydrologic behavior, or hydrologic phenomena in a larger watershed, being more stable than that in a smaller watershed. As a consequence, the simulated results of downstream plain watershed is more accurate than those of upstream reservoir watershed.

7. Concluding Remarks

(1). The concept of the manifold cell model is based on dividing a watershed into several adequate subareas or cells according to topography and streamflow orientation. Linear reservoirs can be analogized to simulate the overland flow and channel flow. Characteristics of spatial variation of runoff process can be revealed in the manifold cell model if an average burst of rainfall falls on a watershed. The resulting runoff hydrograph at the outlet of a river basin can be obtained by convolutional integration from upstream to downstream based upon cell diagram of the actual river basin.

(2) The impulse response function (*IRF*) for the manifold cell model is derived systematically. When the number of zones n becomes infinite, *IRF* of the manifold cell model can achieve reasonable figure similar to the functional shape of a hydrograph. In practical applications, $n \geq 10$ is acceptable for a moderate size watershed zoning.

(3) ARX routing method was used in this study to the manifold cell models. The ARX shceme is simpler and quicker in calculation than convolution. Another important advantage is that the ARX method can be linked to Kalman filter. That is why the manifold cell model is a powerful distributed hydrologic model fit to be extensively employed in flood prediction and prevention.

(4) The criteria of objective function adopted are very important for evaluating the adequacy of a hydrologic model. To meet the requirements of hydrologic design and planning, a bilateral objective function of considering both hydrograph pattern and peak discharge was used in this study. Also for determining accurately and efficiently the parameters used in the manifold cell model, the method of the steepest descent was adopted for parameter optimization.

(5) From the simulated results of the historical typhoon events in the project river basin, the results of the manifold cell model were almost satisfactory.

(6) Adding some boundary conditions into a hydrologic model sometimes becomes a difficult task when model building. Spilling-water condition of a reservoir during typhoon-hitting period was incorporated into the manifold cell model in this study. From the simulated results of Typhoon Billie, manifold cell model accurately revealed the effect of spilling water to the downstream plain watershed. This may be regarded as one of the important advantages of the manifold cell model when applied to a comprehensive reservoir project area such as Tseng-wen River Basin, Taiwan.

(7) Linking the manifold cell model to Kalman filter for flood prediction of 1, 2 and 3 hours ahead, the predicted results were rather satisfactory. Flood prediction for longer time intervals may need more detailed modification.

References

1) Bras Rafael L. and Tgnacio Rodriquez-Iturbe, *Random Function and Hydrology*, Addison-Wesley Publishing Company, 1985.
2) Chow, V. T, ed., *Handbook of Applied Hydrology*, Mc Graw-Hill Book Co., 1964.
3) Chow, V. T., D. R. Maidment and L. W. Mays, *Applied Hydrology*, Mc Graw-Hill Book Co., 1988.
4) Diskin, M. H. and G. G. S. Pegram, "A Study of Cell Models, 3. A Pilot Study on the Calibration of Manifold Cell Models in the Time Domain and in the Laplace Domain," Water Resources Research, Vol. 23, No. 4, 1987.
5) Gerald, C. F. and P. O. Wheatley, *Applied Numerical Analysis*, Taipei Book Co., 1986.
6) Ishihara, Yasuo and Shigeki Kobatake, "Runoff Model for Flood Forecasting," Bulletin of Disaster Prevention Research Institute, Kyoto University, Vol. 29, Part 1, No. 260, July, 1979.
7) Mein, R. G., E. M. Laurenson and T. A. MacMahon, "Simple Nonlinear Method for Flood Estimation," J. of Hydraulics, Div. ASCE, Vol. 100, No, HY 11, 1974.
8) Pegram, G. G. S. and M. H. Diskin, "A Study of Cell Models, 1. A Manifold Cell Model for Distributed Surface Runoff Systems," Water Resources Research, Vol. 23, No. 4, 1987.
9) Pegram, G. G. S. and M. H. Diskin, "A Study of Cell Models, 2. The Effect Time Delay on the Limiting Forms of Cascade and Manifold Cell Model Response Functions," Water Resources Research, Vol. 23, No. 4, 1987.
10) Takasao, Takuma, Michiharu Shiiba and Yasuto Tachikawa, "A Topographic Basin Model for Building a Distributed Rainfall-Runoff Model," Annuals of Disaster Prevention Research Institute, Kyoto University, No. 34 B-2, 1991.
11) Wang, Ru-yih and Jen Yih, *Applied Hydrology*, National Editorial Office, ROC, 1979.
12) Wang, Ru-yih and Kuan-tun Lee, "Study of the Geomorphologic Instantaneous Unit Hydrograph and Its Application," Proceedings of Fifth Congress Asian and Pacific Regional Division, International Association for Hydraulic Research, Seoul, Republic of Korea, August, 1986.
13) Wang, Ru-yih and Chen-her Jean, "A Study on Rainfall-Runoff Models of Watersheds along Hsin-tien Creek, Tan-shui River Basin," Proceedings of the ROC-Japan Joint Seminar on Multiple Hazards Mitigation, National Taiwan University, Taipei, ROC, 1987.
14) Wang, Ru-yih and Rong-wei Lee, "Theoretical Analysis of the Cell Model and Its Application to Flood Routing in a River Basin," Journal of Chinese Agricultural Engineering, Vol. 35, No. 4, December, 1989.
15) Wismer, David A. and R. Chattergy, *Introduction to Nonlinear Optimization*, Central Book Publishing Co., 1981.